

ICARUS: A Specialized Architecture for Neural Radiance Fields Rendering

CHAOLIN RAO, ShanghaiTech University, China and GGU Technology Co., Ltd., China

HUANGJIE YU, ShanghaiTech University, China

HAOCHUAN WAN, ShanghaiTech University, China

JINDONG ZHOU, ShanghaiTech University, China

YUEYANG ZHENG, ShanghaiTech University, China

MINYE WU, KU Leuven, Belgium

YU MA, ShanghaiTech University, China

ANPEI CHEN, ShanghaiTech University, China

BINZHE YUAN, ShanghaiTech University, China

PINGQIANG ZHOU, ShanghaiTech University, China

XIN LOU*, ShanghaiTech University, China and GGU Technology Co., Ltd., China

JINGYI YU*, ShanghaiTech University, China

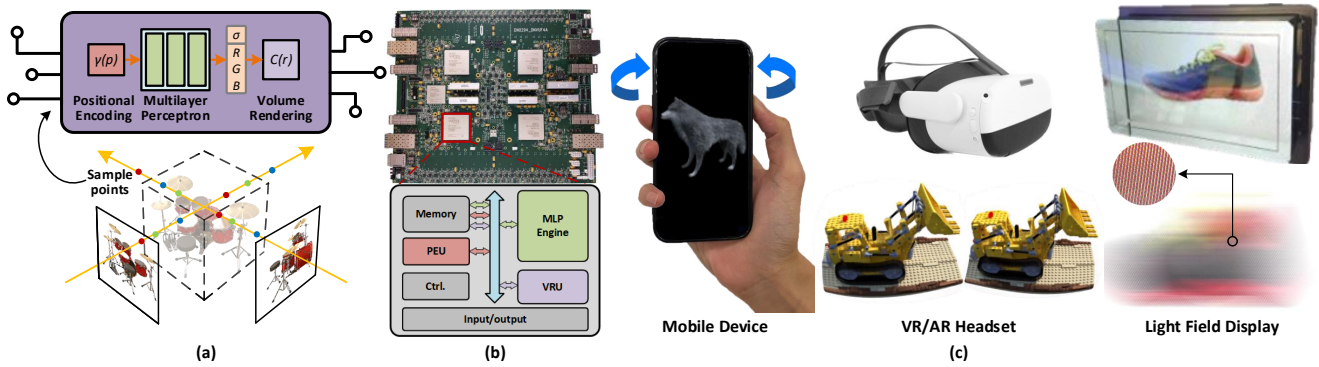


Fig. 1. We demonstrate a specialized hardware architecture for NeRF-based rendering applications. (a) Our hardware design involves operations in NeRF-based rendering. (b) We validate our architecture using an FPGA platform. (c) Potential applications that can benefit from our architecture.

*Corresponding author.

Authors' addresses: Chaolin Rao, raocl@shanghaitech.edu.cn, ShanghaiTech University, Shanghai, China and GGU Technology Co., Ltd., China; Huangjie Yu, yuhj@shanghaitech.edu.cn, ShanghaiTech University, Shanghai, China; Haochuan Wan, wanhc@shanghaitech.edu.cn, ShanghaiTech University, Shanghai, China; Jindong Zhou, zhoujd@shanghaitech.edu.cn, ShanghaiTech University, Shanghai, China; Yueyang Zheng, zhengyy1@shanghaitech.edu.cn, ShanghaiTech University, Shanghai, China; Minye Wu, minye.wu@kuleuven.be, KU Leuven, Belgium; Yu Ma, mayu@shanghaitech.edu.cn, ShanghaiTech University, Shanghai, China; Anpei Chen, chenap@shanghaitech.edu.cn, ShanghaiTech University, Shanghai, China; Binzhe Yuan, yuanbzh@shanghaitech.edu.cn, ShanghaiTech University, Shanghai, China; Pingqiang Zhou, zhoupq@shanghaitech.edu.cn, ShanghaiTech University, Shanghai, China; Xin Lou, louxin@shanghaitech.edu.cn, ShanghaiTech University, Shanghai, China and GGU Technology Co., Ltd., China; Jingyi Yu, yujingyi@shanghaitech.edu.cn, ShanghaiTech University, Shanghai, China.

Permission to make digital or hard copies of part or all of this work for personal or classroom use is granted without fee provided that copies are not made or distributed for profit or commercial advantage and that copies bear this notice and the full citation on the first page. Copyrights for third-party components of this work must be honored. For all other uses, contact the owner/author(s).

© 2022 Copyright held by the owner/author(s).

0730-0301/2022/12-ART234

<https://doi.org/10.1145/3550454.3555505>

The practical deployment of Neural Radiance Fields (NeRF) in rendering applications faces several challenges, with the most critical one being low rendering speed on even high-end graphic processing units (GPUs). In this paper, we present ICARUS, a specialized accelerator architecture tailored for NeRF rendering. Unlike GPUs using general purpose computing and memory architectures for NeRF, ICARUS executes the complete NeRF pipeline using dedicated plenoptic cores (PLCore) consisting of a positional encoding unit (PEU), a multi-layer perceptron (MLP) engine, and a volume rendering unit (VRU). A PLCore takes in positions & directions and renders the corresponding pixel colors without any intermediate data going off-chip for temporary storage and exchange, which can be time and power consuming. To implement the most expensive component of NeRF, i.e., the MLP, we transform the fully connected operations to approximated reconfigurable multiple constant multiplications (MCMs), where common subexpressions are shared across different multiplications to improve the computation efficiency. We build a prototype ICARUS using Synopsys HAPS-80 S104, a field programmable gate array (FPGA)-based prototyping system for large-scale integrated circuits and systems design. We evaluate the power-performance-area (PPA) of a PLCore using 40nm LP CMOS technology. Working at 400

MHz, a single PLCore occupies 16.5 mm^2 and consumes 282.8 mW, translating to 0.105 uJ/sample. The results are compared with those of GPU and tensor processing unit (TPU) implementations.

CCS Concepts: • **Hardware** → **Integrated circuits**; *Very large scale integration design*.

Additional Key Words and Phrases: Neural radiance fields (NeRF), Neural rendering, hardware accelerator

ACM Reference Format:

Chaolin Rao, Huangjie Yu, Haochuan Wan, Jindong Zhou, Yueyang Zheng, Minye Wu, Yu Ma, Anpei Chen, Binzhe Yuan, Pingqiang Zhou, Xin Lou, and Jingyi Yu. 2022. ICARUS: A Specialized Architecture for Neural Radiance Fields Rendering. *ACM Trans. Graph.* 41, 6, Article 234 (December 2022), 14 pages. <https://doi.org/10.1145/3550454.3555505>

1 INTRODUCTION

Advances on computer graphics algorithms are often trailed by their adoptions by hardware. Classic examples range from earlier z-buffer [Catmull 1974] for depth sorting [Newell et al. 1972], to geometry shaders [Bailey 2007] for realizing various subdivision schemes [Akenine-Möller et al. 2019; Han 2007; Kazakov 2007], and to tailored microarchitectures (RDNA2 of AMD and Ampere of NVIDIA) [hardware 2020; Nvidia 2020] for accelerating ray tracing [Meister et al. 2021; Sanzharov et al. 2020]. With their focus anchored at producing physically correct rendering, latest hardware solutions still struggle to strike an intricate balance between real-time performance and high photorealism, especially for applications that can only afford lightweight graphics architecture.

Recent neural rendering approaches provide an alternative, generation oriented solutions to traditional physical simulation. The seminal work of Neural Radiance Fields (NeRF) [Mildenhall et al. 2020] implicitly reproduces the complete plenoptic function, i.e., the radiance along every ray, from sampled rays via tailored deep networks. The idea can be traced back to image-based modeling and rendering (IBMR) that first stores a set of captured photographs as a ray database and then employs tailored interpolation schemes to reconstruct the plenoptic function for view synthesis. Earlier IBMR techniques faced hurdles on both rendering quality and speed. For example, as occlusions between scene objects are inherently discontinuous and hence difficult to interpolate, they can cause severe aliasing artifacts unless ultra-dense ray samples are captured or highly accurate geometry is accessible, both prohibitively difficult under practical settings. In addition, storing ray samples as textures leads to excessive texture memory access at the rendering stage, limiting the performance of modern GPUs.

To mitigate the occlusion problem, NeRF employs a volume rendering model that first estimates density (occupancy) changes along each ray and then aggregates the color accordingly. It uses a multi-layer perceptron (MLP) neural net to reconstruct, store, and query the complete radiance field. In fact, its MLP-based representation serves as a de facto compressor and interpolant: the standard NeRF uses around 1,200,000 parameters of a total size 4.6MB to provide a continuous representation of the radiance field. A key bottleneck of NeRF is training the network. Various acceleration schemes have emerged based on tailored data structures [Liu et al. 2020; Yu et al. 2021a,b], smart training strategies [Deng et al. 2022; Sun et al. 2021], and hardware features on graphics architecture [Müller et al. 2022],

reducing training time from hours to seconds. Reduction of training time comes at the cost of high space usage where advanced and expensive graphics hardware is required to store the intermediate data to enable real-time rendering.

In this paper, we present ICARUS, a specialized architecture tailored for MLP-oriented neural rendering such as NeRF. GPUs use general purpose architectures for the computation of MLP and other neural rendering steps, along with additional components and off-chip memory for storing and exchanging intermediate data. ICARUS, in contrast, uses dedicated plenoptic cores (PLCore) as key computation components to execute the complete volume rendering pipeline without off-chip data exchanges and temporary storage. Each PLCore consists of a positional encoding unit (PEU), an MLP engine, and a volume rendering unit (VRU). It takes in positions & directions and outputs the corresponding pixel colors with all computation and storage on-chip. This allows ICARUS to implement NeRF rendering in high parallelism with little overhead of control and off-chip memory access, significantly reducing time and power consumption. In particular, for MLP computation, we transform the fully connected operations to approximated reconfigurable multiple constant multiplications (RMCs). This further leads to about 1/3 hardware complexity reduction compared to conventional multiply-accumulate (MAC)-based approaches.

We demonstrate a prototype single-core version ICARUS using Synopsys HAPS-80 S104, a field programmable gate array (FPGA)-based prototyping system for large-scale integrated circuits and systems. We evaluate the power-performance-area (PPA) of a PLCore using 40nm LP CMOS technology. Working at 400 MHz, a PLCore occupies 16.5 mm^2 and consumes 282.8 mW, translating to 0.105 uJ/sample. Apart from the original NeRF, we also evaluate implicit signed distance function (SDF) on ICARUS, to extract 3D geometry from the trained MLP via isosurface polygonisation for subsequent geometry processing tasks, useful in both 3D object scanning and other applications such as computerized tomography (CT) and magnetic resonance imaging (MRI) visualizations. With known 3D geometry, we also demonstrate bypassing the radiance aggregation component in ICARUS to directly conduct surface light field (SLF) rendering. We also develop tailored instructions for ICARUS to support NeRF rendering on a variety of displays. As a lightweight architecture, ICARUS aims to enable the displays to "fly" without tethering them to a mainframe and at the same time reduce the power consumption to avoid being "burned", critical for future immersive experiences.

2 RELATED WORK

ICARUS, as an academic prototype, aims to provide a dedicated architecture for neural radiance fields rendering. In many ways, it follows the footstep of the ray tracing hardware that started with a well studied algorithm and eventually landed to the hardware, with strong support from both academia and industry. As a neural rendering architecture, ICARUS also borrows design strategies from deep neural network chips to balance between power, memory, and bandwidth. In this section, we discuss the most relevant works in respective fields.

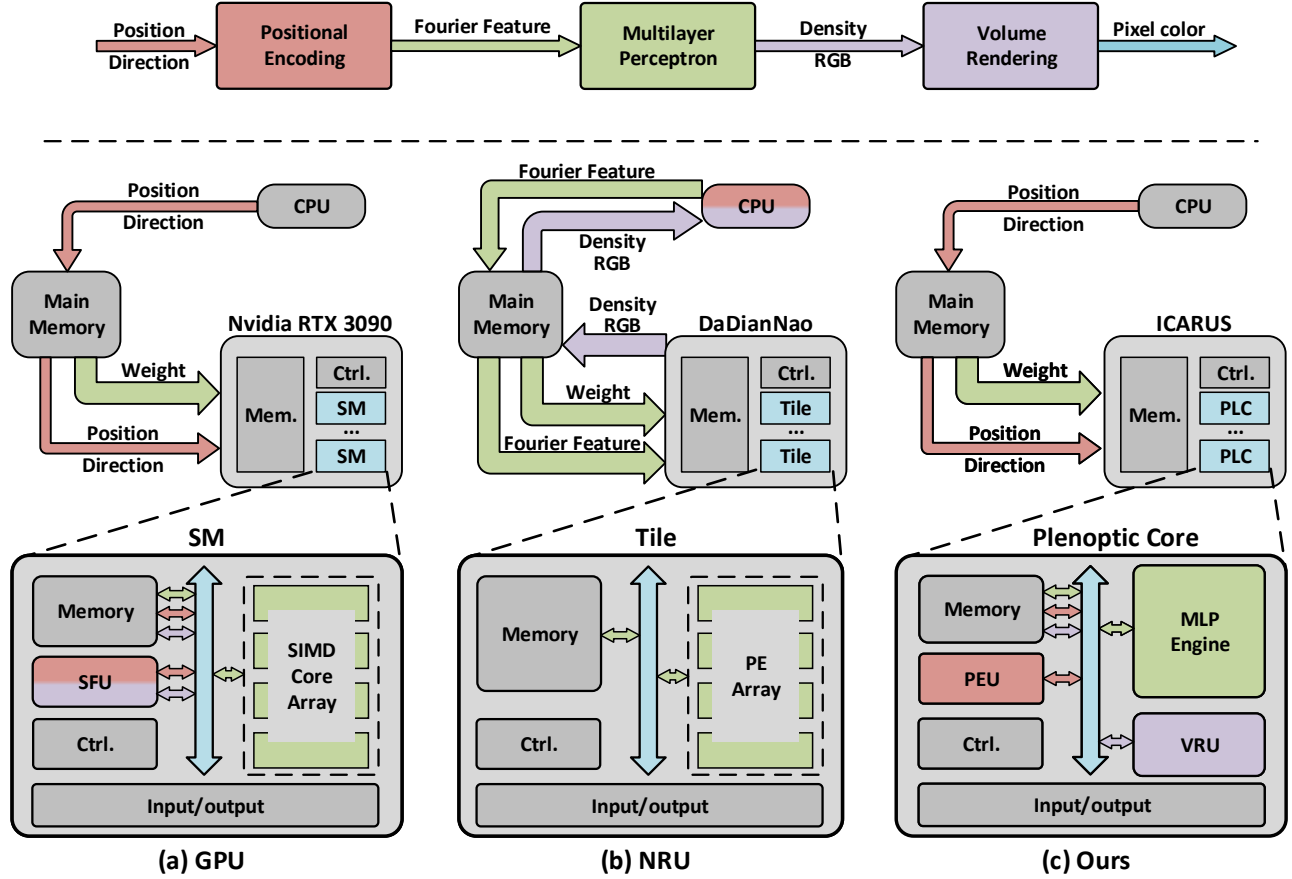


Fig. 2. Illustration of mapping NeRF to (a) GPU (b) NPU and (c) ICARUS. For GPU-based NeRF implementation, positional encoding and volume rendering are executed in the SFU, and MLP is mapped to SIMD core arrays. Intermediate data is exchanged using off-chip memory. For NPU-based NeRF implementation, positional encoding and volume rendering are executed in CPU and MLP is mapped to PE arrays. Intermediate data is also exchanged using off-chip memory. ICARUS executes the complete NeRF pipeline using dedicated plenoptic cores (PLCore) consisting of a PEU, an MLP engine, and a VRU.

Ray Tracing Hardware. Dedicated graphics hardware has unexceptionally come from its academic prototypes. Earlier volume rendering accelerator had been under heavy research in academia before powerful GPUs became accessible from industry. The Volume-Pro system [Pfister et al. 1999] focused on accelerating ray casting whereas its followup efforts were largely devoted to customizing ray-tracing hardware. Among them, one of best recognized academic breakthrough is SaarCOR (Saarbrücken’s Coherence Optimized Ray Tracer) [Schmittler et al. 2002], an FPGA-based prototype ray-tracing accelerator, which was later extended to the programmable Ray Processing Unit (RPU) [Woop et al. 2005] and the Dynamic Ray Processing Unit (DRPU) [Woop 2007] on products. Academic results have further inspired various microarchitectures based solutions by the GPU industry to achieve near real-time performance [Nah et al. 2015; Spjut et al. 2009] as well as to maintain energy-efficiency on mobile devices [Kim et al. 2012, 2013; Nah et al. 2014, 2011]. They have all eventually landed on today’s high-end commercial GPUs in the form of dedicated ray tracing cores, from

NVIDIA’s RTX series to AMD’s RDNA architecture, and to Imagination Technologies’ mobile PowerVR Photon. The development of ICARUS in this paper hopes to continue this legacy of technology transformation, stemming from academic prototypes and landing on industrial product, but this time in neural rendering.

Neural Network Accelerators. Neural networks, especially convolutional neural networks (CNNs), are widely used in many machine learning applications. The seminal Tensor Processing Unit (TPU) [Jouppi et al. 2017] from Google adopts a systolic array based design. While its first generation had merely focused on inference tasks (so is ICARUS), later TPU generations, i.e., TPUv2, support both training and inference, showing numerous successes in science and engineering. In fact, TPU is general enough to directly support neural rendering tasks such as NeRF [Deng et al. 2020]. However, even with multiple TPUs, brute-force implementation cannot yet reach real-time performance (0.35 seconds per frame, with 128 TPUv2). Our goal is to develop a tailored rather than general architecture like the TPU.

Light weight neural network solutions have also been extensively studied in the past decade, e.g., DianNao [Chen et al. 2014a] and its subsequent extensions [Chen et al. 2014b; Du et al. 2015; Liu et al. 2015], Eyeriss [Chen et al. 2017] and the follow-up work Eyeriss v2 [Chen et al. 2019], and the Thinker [Yin et al. 2018a,b,c] series, etc. Existing CNN accelerators have mainly focused on data flow optimization to eliminate, at least partially, the bottleneck caused by data movement [Chen et al. 2014a, 2017]. They also emphasize more on the optimization of the convolution operation where a kernel is often convolved with different parts of input feature maps and a specific part of a feature map is convolved with different kernels. Therefore, the architecture design has mainly focused on weight sharing and/or activation strategies [Jo et al. 2018; Moons and Verhelst 2017; Yin et al. 2018a] for improving the performance and at the same time reducing power consumption. For neural radiance fields rendering, whether in its original NeRF version or in consecutive optimized accelerated versions [Müller et al. 2022], fully-connected MLPs instead of CNNs serve as the backbone. Since MLPs are fully connected, a weight is multiplied with only one input neuron and a neuron is multiplied with only a set of weights. Therefore, directly mapping MLP-based rendering scheme to existing CNN accelerators causes efficiency degradation since the computation patterns are different. Fig. 2(b) illustrates the mapping of NeRF's MLP to a CNN accelerator architecture (DaDianNao [Chen et al. 2014b] in this case).

Algorithm-level Optimizations. Our ICARUS prototype follows largely the pure MLP design as in the original NeRF. The earliest version of NeRF was implemented on NVIDIA's GPU. Fig. 2(a) illustrates running NeRF on GPUs. However, as a general purpose computation platform with high power consumption (350 W for NVIDIA RTX 3090), GPU still cannot achieve real-time performance.

A number of algorithm-level techniques have been proposed to accelerate rendering and in some cases training of NeRF [Garbin et al. 2021; Müller et al. 2022; Yu et al. 2021a,b]. These approaches adopt a hybrid representation where the space is partitioned into voxels with well-designed data structures to reduce MLP layers (e.g., down to 2) to accelerate sampling fetching. [Luo et al. 2021] leverages coarse explicit scene geometry priors to guide point sampling along with rays and hence reduce network inference computation whereas [Liu et al. 2020] uses Octree in its hybrid representation to avoid redundant MLP queries in free space. [Garbin et al. 2021] compactly caches a deep radiance map from trained MLPs in voxels, preventing network inference. Similarly, [Yu et al. 2021a] and [Yu et al. 2021b] realize view-dependent effects by adopting spherical harmonics and store coefficients on a sparse voxel grid or an Octree structure respectively. KiloNeRF [Reiser et al. 2021] uses thousands of tiny MLPs to represent parts of the scene so as to reduce the cost of network queries for sample points. Although effective, these techniques unanimously rely on the GPU features for trading space for time and therefore require very large storage (1.9GB for PlenOctrees). Perhaps the most exciting advance is Instant-NGP [Müller et al. 2022] which adopts a multi-resolution encoding scheme coupled with voxel hashing and manages to simplify the original deep MLP to a compact one, reducing training time from hours to seconds and achieving real-time rendering. Nonetheless, its reliance

on GPU hardware features is more extensive. Our pure MLP-based ICARUS provides an alternative solution to achieve high performance rendering without the GPU reliance where concurrent and future extensions may be implemented with proper extensions.

3 DESIGN PHILOSOPHY

3.1 Computation Analysis

This section analyzes the computation in NeRF-based rendering tasks. NeRF implicitly models a continuous plenoptic function $F_{NeRF} : (\mathbf{p}, \mathbf{d}) \rightarrow (\mathbf{c}, \sigma)$ with an MLP, which is trained using a set of images with known poses. By querying the MLP at a position $\mathbf{p} \in \mathbb{R}^3$ from a specific unit-norm viewing direction $\mathbf{d} \in \mathbb{R}^2$, the corresponding density σ and view-dependent color \mathbf{c} at that position can be recovered. To render a pixel, a number of 3D positions, denoted by $(\mathbf{p}_1, \mathbf{p}_2, \dots, \mathbf{p}_N)$, are sampled along the ray that passes through the pixel. The plenoptic function F_{NeRF} has to be evaluated for each sample point \mathbf{p}_i to generate the corresponding color \mathbf{c}_i and density σ_i . Direct volume rendering [Kajiya and Von 1984] is then applied to generate the color of the pixel.

As we can calculate, to render an image with millions of pixels, the plenoptic function F_{NeRF} is evaluated N times for each pixel, translating to tens or even hundreds of millions of MLP queries depending on the number of N . For illustration, the original NeRF samples 192 points along each ray. To render an 800×800 image, the MLP has to be queried $800 \times 800 \times 192 = 122880000$ times. This is the reason why it takes seconds to render a single frame even on modern high-end GPUs.

The evaluations of MLP for different sample points are independent of one another. This means that they can be paralleled to improve the rendering speed, given sufficient computing resources. Parallel processing can be performed on the sample point-level or pixel (ray)-level. In addition, though not very critical in terms of computation, there are another two important steps in the NeRF-based pipeline: positional encoding which transforms positions & directions into a higher dimensional feature space and volume rendering which integrates the colors of sample points to render the final pixel color. Due to the dimension increment, the amount of data for positions and directions is expended by 20 times and 8 times (for the original NeRF), respectively, after positional encoding. For example, to render an 800×800 image with 192 sample points, we only need to load in $800 \times 800 \times 192 \times 6 \times 2B \approx 1.37$ GB if we include positional encoding in our system other than 19.22 GB if we do not (2 Bytes for each input data in our calculation). On the contrary, volume rendering compresses the amount of data by integrating the colors and densities of all sample points to generate the RGB values of the rendering pixels. For the fine rendering step with 128 sample points, the amount of data for an image from the MLP is about $800 \times 800 \times 128 \times 4 \times 2B \approx 625$ MB, which reduces to 3.66 MB after volume rendering.

3.2 Design Decisions

In this section, we present the design decisions for ICARUS. The first and most important decision is to finish the entire NeRF pipeline in a single PLCore without any intermediate data going off-chip for temporary storage and exchange, so as to save computation time and

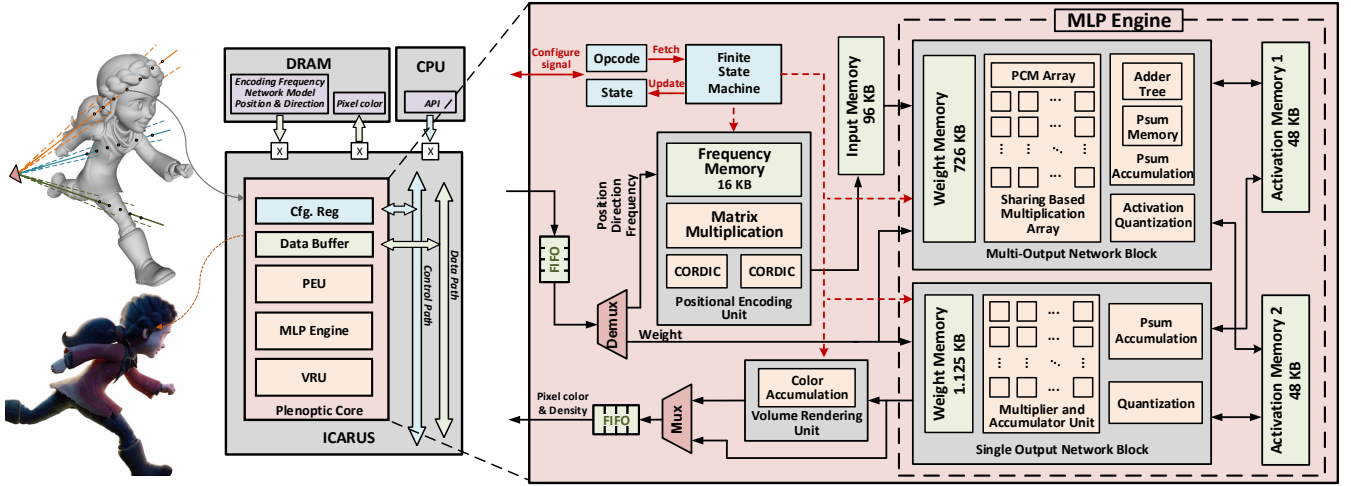


Fig. 3. Overall architecture of the proposed ICARUS. The main computation components in ICARUS is PLCore. For NeRF rendering, a batch of sample points are processed by the PLCore, where the whole NeRF pipeline for a ray is completed inside the PLCore, i.e., a PLCore takes in positions & directions and renders the corresponding pixel colors without any intermediate data going off-chip for temporary storage and exchange.

power consumption. To achieve this, we need to design a dedicated architecture which takes in positions & directions and outputs final pixel colors. Moreover, though NeRF-based rendering algorithms share the same general flow consisting of positional encoding, MLP and volume rendering, they may differ in specific implementation of each module. Therefore, the dedicated architecture needs to have the flexibility to support different implementations of these modules.

Another decision is to optimize the implementation of MLP for computational complexity reduction. Therefore, we use fixed-point instead of floating-point in ICARUS. It is well-known that floating-point computations are generally more complex than their fixed-point counterparts. Since NeRF is computationally demanding, it is very hard, if not impossible, to meet the performance and energy-efficiency requirement for mobile applications using floating-point computation. Apart from fixed-point computation, the fault-tolerant property of neural networks can be utilized to further reduce the computational complexity of NeRF.

4 SYSTEM DESIGN

4.1 Overall System Architecture

Fig. 3 illustrates the overall architecture of ICARUS. For a rendering system consisting of CPU, dynamic random access memory (DRAM) and ICARUS, the inputs, i.e., network model, encoding frequency and positions & directions are stored in DRAM and fed to ICARUS under the control of CPU during runtime. An on-chip network is used to dispatch input data to the destination PLCore. After loading the network model, positions & directions are continuously streamed into ICARUS for NeRF processing and final rendered pixel colors are streamed out through the data path. Inside ICARUS, the sample points of a cluster of rays, comprising a sample point batch, are processed by the same PLCore, where the whole NeRF pipeline is completed inside the PLCore without any intermediate data going off-chip for temporary storage and exchange.

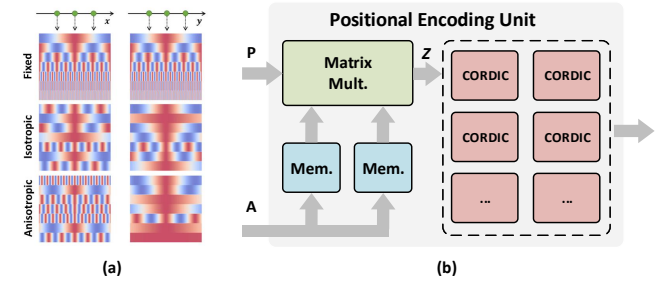


Fig. 4. (a) Three different types of frequency patterns. (b) Overall structure of the PEU. (A: Frequency matrix. P: Input positional data matrix. Z: Results of the matrix multiplication of AP)

The detailed structure of a PLCore is illustrated in the right half of Fig. 3. According to the NeRF pipeline, we design a PLCore consisting of a PEU, an MLP engine and a VRU, where specific rendering steps are executed by the corresponding dedicated hardware module. The PEU transforms the input positions & directions into higher dimensional feature space based on the input encoding frequencies. The encoded positions & directions are fed to the MLP engine to render the colors $c = (r, g, b)$ and densities σ of the sample points, which are further consumed by the VRU to generate the final pixel colors. On-chip static random access memory (SRAM) blocks are used for temporary storage of weights, input positions & directions and intermediate activations during the runtime. The execution of the NeRF pipeline on a PLCore is controlled by the internal finite state machine based on the input processing instructions.

4.2 Positional Encoding Unit

Previous researches have revealed that the feed-forward neural networks tend to learn low frequency signals [Mildenhall et al. 2020;

Rahaman et al. 2019; Zhong et al. 2019], leading to over-blurred rendered images. One technique to overcome such difficulty is to map raw input coordinates into a relatively higher dimensional feature space through Fourier features mapping as

$$\phi(x; A) = [\cos A^T x, \sin A^T x] \quad (1)$$

This procedure is called positional encoding in NeRF-based neural rendering. Afterward, a neural network takes in transformed features instead of raw coordinate vectors.

It is easily perceived that the selection of the frequency matrix A is critical for tuning the smoothness of network outputs. Shown in Fig. 4(a) are different features (frequency matrices) used in different neural rendering algorithms, e.g., fixed frequency for NeRF rendering, isotropic random Fourier features for encoding implicit geometries [Tancik et al. 2020], and anisotropic random Fourier features for neural image-based rendering of implicit geometries [Yu et al. 2022].

In ICARUS, we develop a universal PEU for computing different kinds of feature mapping functions. Fig. 4(b) illustrates the architecture of the PEU in a PLCore. The frequency matrix A , which is the same for all sample points in a particular rendering task, is stored in local memories. During the runtime, positions & directions are streamed into the matrix multiplication unit, in which they are multiplied with the frequency matrix A in a pipelined manner. The resultant intermediate vector z is further fed to the Coordinate Rotation Digital Computer (CORDIC) array to generate the final transformed features, i.e., $\sin(z)$ and $\cos(z)$.

We design PEU to meet the requirement of inner product operations with two different sizes, i.e., (\mathbb{R}^3 and \mathbb{R}^6), for different positional encoding algorithms. For the case of \mathbb{R}^3 , both frequency matrix data and position & direction data are of 3-dimensional, meaning that one block memory with size 3×128 is enough to store the frequency matrix. For the inner product computation, a 3-stage cascaded MAC unit is used to perform three multiplications and two additions in serial. For the case of \mathbb{R}^6 , instead of doubling the size of memory to 6×128 to maintain the same performance, we use two separate 3×128 memory blocks. Since two memory blocks can be accessed independently, the normal \mathbb{R}^3 frequency matrix or the first half of the \mathbb{R}^6 frequency matrix is loaded into the first memory block, and the other memory block stores only the second half of the \mathbb{R}^6 frequency matrix. In \mathbb{R}^6 computation mode, two memory blocks work simultaneously. While in \mathbb{R}^3 computation mode, the second memory is set to a sleep mode for power reduction. Moreover, the inner product results go through all 6 stages of the cascade MAC during \mathbb{R}^6 computation, while in \mathbb{R}^3 calculation, the later 3 stages are bypassed.

4.3 MLP Engine

In the NeRF pipeline, the MLP is the most computation intensive component because tens of millions of MLP query leads to tremendous amount of MAC operations. Therefore, we design a dedicated MLP engine to accelerate the computation of MLP. A typical MLP layer can be expressed as

$$\mathbf{y} = f(W\mathbf{x} + \mathbf{b}) \quad (2)$$

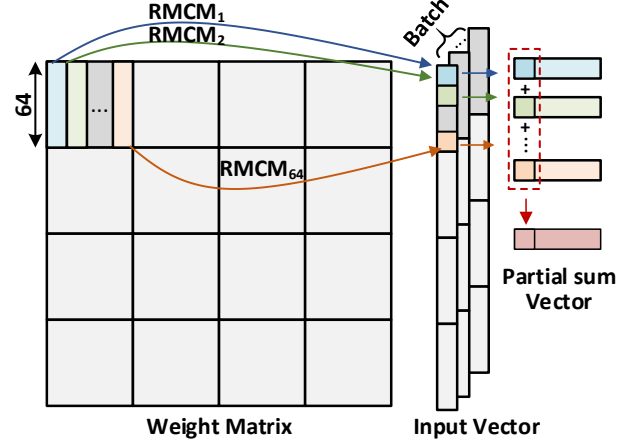


Fig. 5. Overall computation flow in the MLP engine.

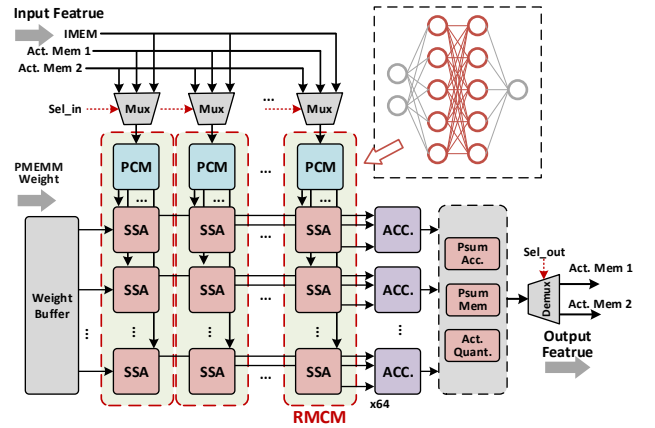


Fig. 6. Computation of matrix-vector multiplication (MVM) using a multiple output network block (MONB).

where \mathbf{x} , W , and \mathbf{b} are the input neuron vector, weight matrix and bias vector, respectively, and f denotes the activation function. As an example, W is a 256×256 matrix in the original NeRF.

The overall architecture of the MLP engine is illustrated in Fig. 3, which consists of a multi-output network block (MONB), a single output network block (SONB) and two activation memory blocks. The MONB block is responsible for the computation of hidden layers in an MLP where multiple output neurons are generated, while the SONB block is designed to compute the output layer of MLPs in NeRF, which generates the density or color of sample points. We design a dedicated SONB block because when mapping the output layer to MONB, most of the computation resources are wasted. We use a MAC array with 64 general multipliers to implement the fully-connected operations in SONB.

Fig. 5 illustrates the overall computation flow in an MLP engine. Instead of using a large matrix-vector multiplication (MVM) block for an entire layer, we partition it into several sub-MVM blocks with sizes of 64×64 , making it more flexible for various NeRF-based

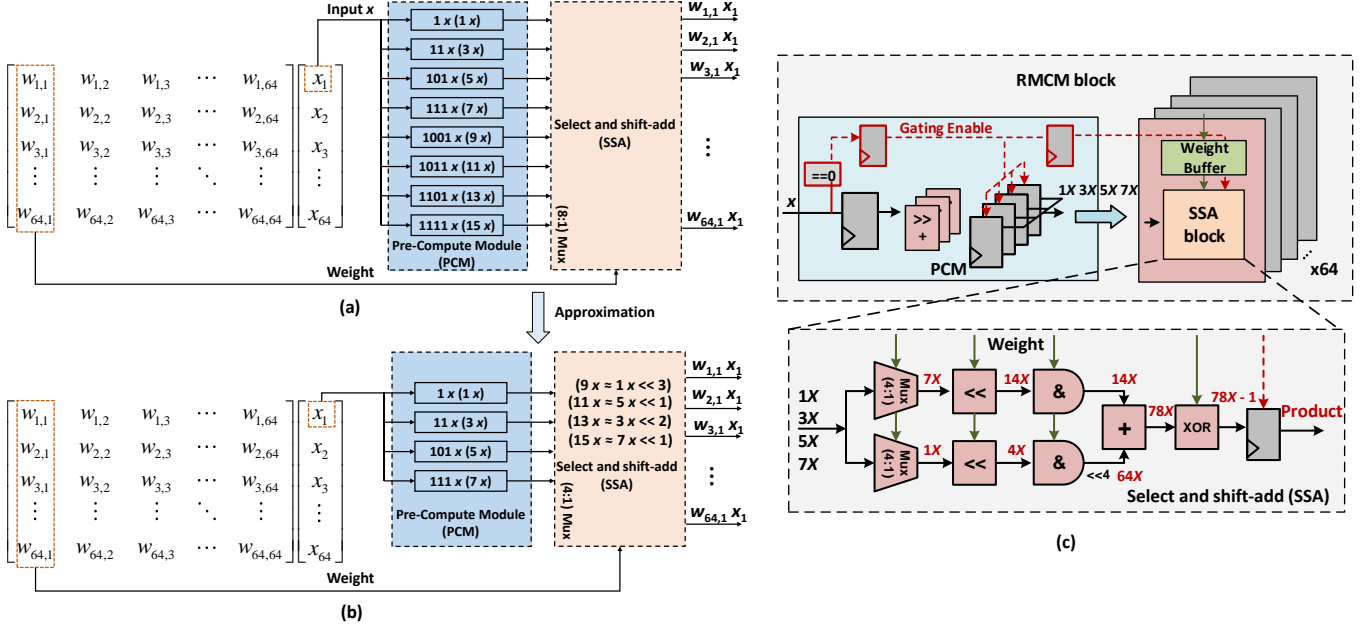


Fig. 7. Working principle of (a) RCMC and (b) approximated RCMC. (c) Detailed implementation of the RCMC block. For approximated RCMC, the second half of common subexpressions are approximated using their nearest neighbors.

rendering tasks with different matrix size (usually multiples of 64). For the implementation of a sub-MVM, taking the top-left block as an example, we transform it into 64 shift-add based reconfigurable multiple constant multiplication (RCMC) operations, where adder trees are further used to compress 64 partial results into the final resultant vector. The advantages of using RCMC are multi-fold. It is faster and more power-efficient than conventional MAC-based implementation since the common subexpressions are shared across different multipliers [Park et al. 2004]. Moreover, we further adopt the idea of batch-computing to reduce off-chip memory access for weights. As illustrated in Fig. 5, after loaded into the sub-MVM block, the weight matrix stays stationary for a certain amount cycles and multiply with a set of input vectors for different sample points. Batch-computing reduces off-chip memory access for weight matrix at the cost of a small extra on-chip memory for intermediate output vectors. In our design, a batch size of 128 sample points are used, i.e., the weight matrix stays stationary in the MLP engine for the computation of sub-MVMs of 128 sample points.

The computation of MVM in Fig. 5 using a MONB block is illustrated in Fig. 6. In our design, a MONB block consists of 64 parallel RCMC blocks, where each RCMC block performs the RCMC operation shown in Fig. 5 with 64 coefficients. The multiplication results of RCMC blocks at the same vertical positions, i.e., in the same row, are summed up by the corresponding adder tree. The summation results from the adder trees are further accumulated in the following block to generate the final MVM results. In particular, three buses load inputs come from the Input Memory, Activation Memory 1 and Activation Memory 2, where each data bus transfers 64 parallel activations. In each cycle, only one of the three data bus is activated by the multiplexers under the control of the Sel_in signal.

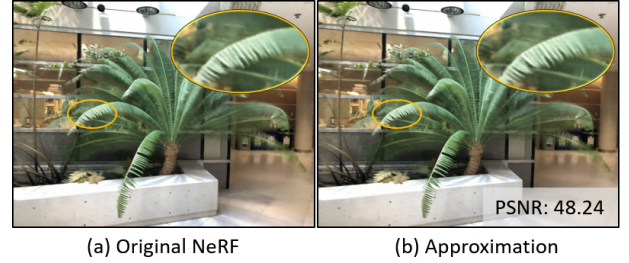


Fig. 8. Two images rendered using (a) the original NeRF and (b) NeRF implemented using approximated RCMC.

The selected data is fed to 64 pre-compute modules (PCMs), where each PCM generates 4 common subexpressions (1x, 3x, 5x and 7x) that shared by the following 64 select & shift-add (SSA) blocks in the same column. Each SSA calculates the approximated product between input an activation and a weight by proper shift-add operations. Along the horizontal direction, the SSA in the same row computes 64 products of the same inner product operation, which are summed up by the adder tree to generate one inner product for the MVM. Once finished, the results of MVM are sent to the activation & quantization (Act. Quant.) module for bias accumulation, activation operation and re-quantization operation. A demultiplexer (Demux) finally chooses the correct activation memory (Activation Memory 1 or Activation Memory 2) to save the output neurons.

Fig. 7(a) illustrates the working principle of the RCMC for MVM computation, which is inspired by the work in [Park et al. 2004]. The basic idea is to pre-compute a set of partial products, usually

referred as common subexpressions, and share them across different multipliers. Since common subexpressions are fixed, they can be implemented using only shift-add operations. For example, $3x$ can be realized using only one shift-add operation as

$$3x = 1x \ll 1 + 1x \quad (3)$$

where " \ll " represents a left-shift operation. In the select & shift-add (SSA) block in Fig. 7(a), multiplexers are used to select the needed common subexpressions according to the value of input weights. The selected common subexpressions are then shifted and summed up to generate the final multiplication results. Let us take a 9-bit weight $-78(1_0100_1110)_2$ represented in the signed-magnitude form as an example. We first divide the weight into two parts, i.e., higher part 0100 and lower part 1110. Two multiplexers in the SSA block choose $1x$ and $7x$ for the higher part and lower part, respectively. Two shifters are then used to shift $1x$ and $7x$ to $0100x(4x)$ and $1110x(14x)$, respectively. Then we shift the result of higher part to the left by 4 bits to get $0100_0000x(64x)$. An adder finally sums up the results of higher part and lower part to produce the final result $78x$.

Since neural networks are naturally fault-tolerant, we further adopt the idea of approximation to the RMCM block for further hardware complexity reduction. As illustrated in Fig. 7(b), the second half of the pre-compute common subexpressions, i.e., $9X$, $11X$, $13X$ and $15X$, are omitted, and the values are approximated with their nearest neighbours. Since the number of common subexpressions is reduced from 8 to 4, the original (8:1) multiplexer is replaced by a (4:1), leading to hardware reduction for circuit implementation. In the meantime, the error introduced by this approximation is small (maximum error is $1/9$ of the original multiplication result), which can be further compensated during the training process. Fig. 8 shows two images rendered using (a) the original NeRF and (b) NeRF implemented using approximated RMCM. As we can see, there is no observable visual difference. The peak signal-to-noise ratio (PSNR) is as high as 48.24. By the introducing of approximation, the circuit area can be reduced by about $1/3$.

Fig. 7(c) illustrates the implementation details of the RMCM block. The pre-compute module generates the four common subexpressions, which are consumed by the following 64 SSA block. A comparator in PCM checks if the input is a zero or not, and gate the products (for zero input) for power-saving. A SSA block takes in the common subexpressions and generates the final multiplication result with proper selection and shift-add operations.

Compared with hidden layers, the computation of output layer is much simpler. In order to keep the same data from Activation Memory 1 and Activation Memory 2 to reduce the complexity of reading control, we implement 64 multiplication units in SONB as shown in Fig. 9. The data flow in SONB is similar to MONB except that the multiplications in SONB are implemented using general multipliers instead of RMCM blocks.

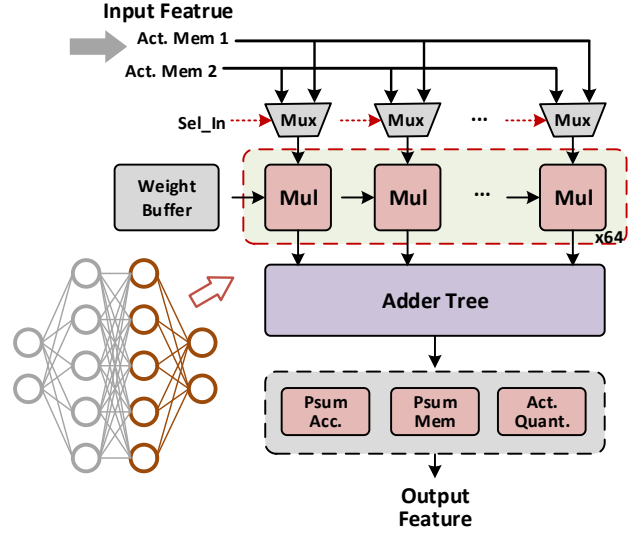


Fig. 9. Detailed structure of the single output network block (SONB). It is used to compute the output layer of an MLP.

4.4 Volume Rendering Unit

In ICARUS, a VRU is implemented to render the final pixel colors. The main motivation of using a dedicated module instead of using CPU for volume rendering is to reduce the off-chip memory access. Since colors and densities of all sample points in a ray are compressed to the color of a pixel after volume rendering, data exchange between ICARUS and main memory is significantly reduced. Take the original NeRF as an example. To perform volume rendering outside ICARUS in a host CPU, we need to output the colors $c = (r, g, b)$ and densities σ of 128 sample points (fine rendering only) for each ray. While after volume rendering, the output data is the color $c = (r, g, b)$ of one pixel, which is only $3/(128 \times 4) \approx 0.586\%$ of that mentioned above.

The classic volume rendering equation [Max 1995; Perlin and Hoffert 1989] is given by

$$C(r) = \sum_{i=1}^N T_i (1 - \exp(-x_i)) c_i, \quad (4)$$

$$T_i = \exp\left(-\sum_{j=1}^{i-1} x_j\right), \quad x_i = -\sigma_i \delta_i$$

where $\delta_i = t_{i+1} - t_i$ is the distance between adjacent samples, $C(r)$ is the color of one ray we estimated by sample points, σ is the volume density calculated by network and c_i is the color of each sample point that goes through the activation function of sigmoid. We can rewrite the formula (4) to

$$C(r) = \sum_{i=1}^N (T_i - T_{i+1}) c_i, \quad (5)$$

$$T_{i+1} = \prod_{j=1}^{i+1} \exp(-x_j) = T_i \cdot \exp(-x_{i+1})$$

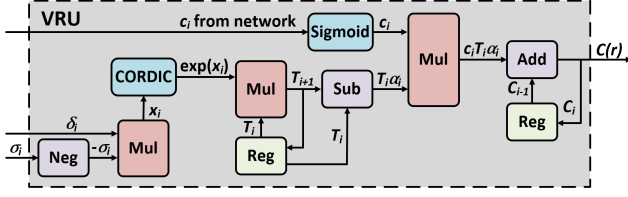
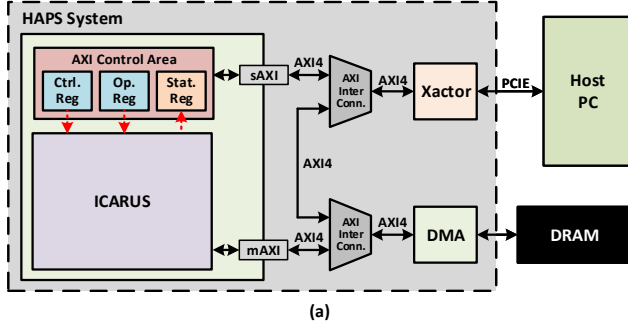
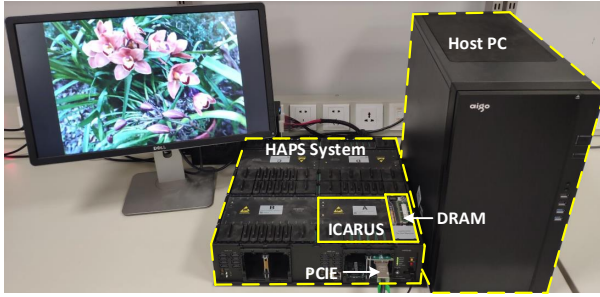


Fig. 10. Detailed structure of the volume rendering unit (VRU).



(a)



(b)

Fig. 11. (a) Block diagram and (b) system setup of the FPGA-based prototype system.

Fig.10 illustrates the architecture of the VRU, which implements the rendering equation (5). In the VRU, we use a CORDIC module to calculate the exponential of x_i . The registered T_i is used in two calculations: 1) the multiplication with $\exp(x_i)$ to get T_{i+1} and 2) the subtraction with T_{i+1} to generate $T_i \cdot \alpha_i$, where $\alpha_i = 1 - \exp(x_i)$. After finishing these two operations, T_i is replaced by T_{i+1} for the calculation in next accumulation. Once we have the coefficient of c_i , we multiply it with c_i to get the weighted color C_i of one sample point. The accumulations proceeds until we get the color of one pixel.

5 VALIDATION AND PERFORMANCE EVALUATIONS

To validate the proposed rendering system, we build a proof-of-concept prototype which implements a single core version ICARUS on Synopsys HAPS-80 S104, an FPGA-based prototype system. Moreover, to evaluate the performance of ICARUS, we also map our design to 40nm CMOS technology. The rendering performance of ICARUS, including the quality of rendered image as well as speed

and energy efficiency, are compared with the GPU and TPU implementations.

5.1 FPGA Prototype

Fig. 11(a) shows the block diagram of the FPGA prototype system, consisting of an ICARUS co-processor for NeRF rendering, a host PC for system control and a DRAM for data exchange between ICARUS and PC. The host PC connects to ICARUS through PCIe bus, where a Synopsys Xactor is used to decode the PCIe stream to AXI format. There are three addressable registers in the prototype system where two of them are write-only registers for saving processing instructions & control signals and the other one is a read-only register for indicating the state of the system. The system setup is illustrated in Fig. 11(b). After loading the network model, the host PC send inputs and instructions to the DRAM on HAPS. The ICARUS co-processor reads the inputs and processing instructions, and executes the NeRF pipeline. The rendered pixel colors are sent back to the host PC to generate the final image. The following evaluation results of NeRF and surface light field (SLF) rendering are performed using the above mentioned FPGA prototype.

Neural Radiance Field Rendering. In our evaluation, for each pixel to render, we adopt a two-pass sampling strategy as in the original NeRF: first generate 64 uniformly distributed samples within the visible range, calculate density distribution along the pixel ray and finally generate another 128 samples that are more close to the surface of the object.

Fig. 12 compares the NeRF rendering results using GPU and ICARUS. Note that we also include the ground truth images for reference. We run comprehensive experiments using both synthetic and real scenes that are presented in previous works. As illustrated, there are practically no visual differences between our results and those generated by GPUs under all scenes. In the ‘ficus’ and ‘fern’ scene, we faithfully preserve fine leaf edges. Likewise, in the ‘ship’ scene, we reproduce the reflectance of water and the thin mast of the ship. These experiments reveal the fact that fixed-point computation is appropriate for rendering tasks and validate the precision of our computing pipeline. They further demonstrate that our hardware is a sensible substitution of GPU in the domain of NeRF rendering.

In terms of quantitative evaluation, we use the commonly used PSNR to measure the quality of rendering results. As we can see, for most cases (especially the real scenes), the PSNRs of GPU results and ICARUS results are very close, where the gap is less than 1dB. But we also note that for certain cases in the synthetic scenes, for example the ‘chair’, the PSNR gap between GPU results and ICARUS results can be as large as 2dB. This gap is caused by the post-training quantization we used in this work, where the weights are linearly quantized without retraining. But according to existing research on network quantization, this PSNR degradation can be alleviated or even complete addressed by some techniques such as quantization aware training [Jacob et al. 2018], which has been widely used in many neural network implementations.

Neural Surface Light Field Rendering. A surface light field (SLF) [Wood et al. 2000] employs a collection of light rays that emit from the surface of an object towards all directions. Like NeRF, each light ray has

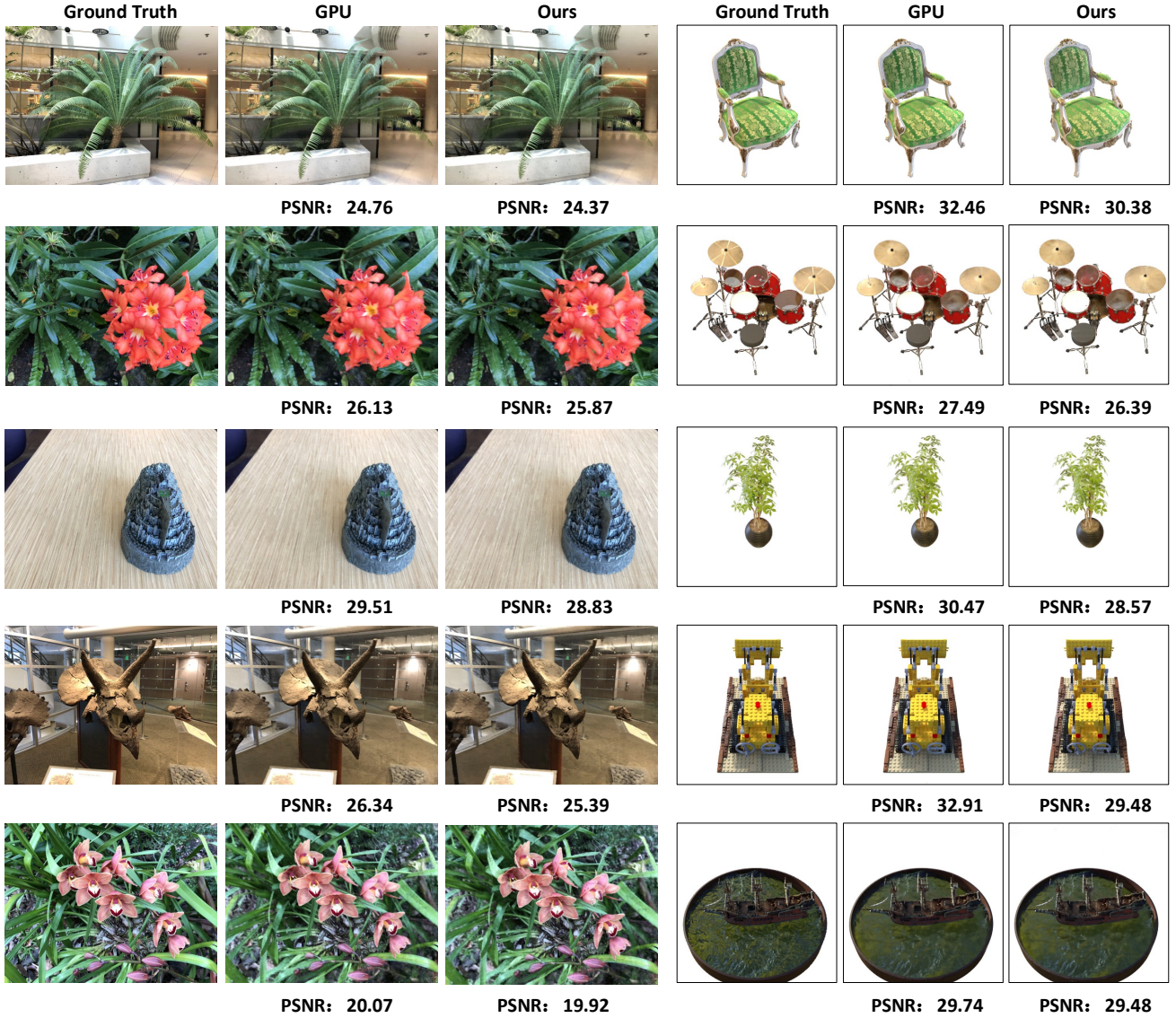


Fig. 12. Comparison of NeRF rendering results using GPU and ICARUS. PSNRs are presented below each result.

an attached radiance value except that they are parametrized over the surface. In that perspective, an SLF serves as an object-level representation of the plenoptic function. Brute-force rendering using an SLF is straightforward: given a virtual camera in the free space, we directly trace view rays from its center of projection towards the surface, compute their interaction points with the scene, and the query SLF via techniques such as the unstructured lumigraph [Buehler et al. 2001]. For high quality rendering, a large number of images (at the same scale of NeRF) are required and hand-crafted blending schemes are essential to reduce visual artifacts.

Analogous to NeRF, deep surface light [Chen et al. 2018] shows that one can also compactly encode an SLF into an MLP as shown

in Fig. 13. Specifically, we leverage MLPs' abilities for providing continuous representations, delegating the interpolation duty to the neural network. Once the network is properly trained, we can treat it as an ordinary continuous function for querying novel radiance. Different from NeRF though, the input to the SLF network for querying the radiance is a six-dimensional vector: it consists of three elements for a spatial point on the object surface, and another three for the angular direction of the virtual ray. It is possible to further employ anisotropic Fourier features [Yu et al. 2022] to enhance view dependency.

We observe that an SLF exhibits strong variations in the spatial domain but low in the angular domain. Therefore we construct

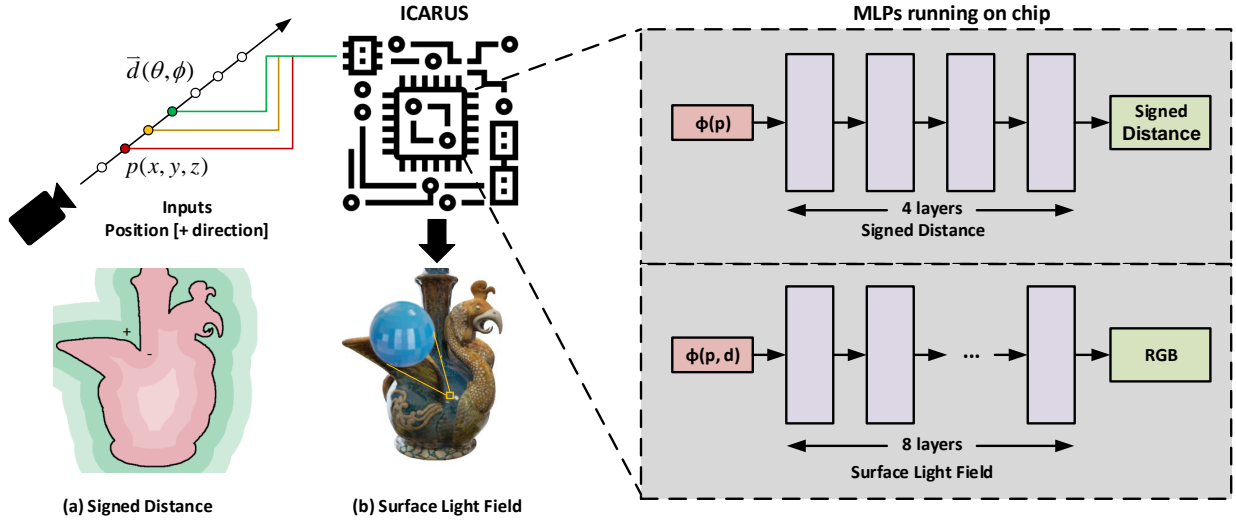


Fig. 13. Computing architectures of (a) neural signed distance field and (b) neural surface light field.

the transformation from two separate smoothing parameters, one for high spatial variance and the other for low angular variance. We use ICARUS to directly implement the corresponding transformations on the chip to reduce data transfers while achieving high performance. Unlike NeRF though, rendering an SLF requires explicit geometry such as a mesh. This indicates that ICARUS will have to interface with a full graphics pipeline, which is difficult to conduct in practice. Therefore, to bypass the GPUs by using the matrix-multiplication-based rendering on ICARUS, we adopt another neural network to handle geometry. Specifically, we use a signed distance function (SDF) network [Park et al. 2019] that can implicitly encode any given mesh surfaces. In a nutshell, the SDF network takes in a spatial point in free space and produces the minimum distance from the point to the surface. Once converted, the SDF can be used to march any virtual ray to locate its intersection point with the surface through iterative evaluation using the SDF network.

To train an MLP-based SLF (on the GPU), we employ the Fourier features to preserve maximum geometry details. Since an SDF is almost uniformly distributed and exhibits small variances across different axes, we use isotropic transformations using a single smoothing parameter. It is worth noting that our neural SLF rendering does not require evaluating a large set of samples along each ray as in NeRF: once we obtain the intersection of any virtual ray with the surface, we only need to evaluate that single sample. Fig. 14 shows a sample comparison between the GPU and the ICARUS for the neural SLF rendering task. Quality wise, both visually and quantitatively (in terms of PSNR), ICARUS achieves a similar performance to its GPU implementation.

5.2 ASIC Evaluation

To evaluate the speed and energy-efficiency of ICARUS, we map ICARUS system to ASIC platform based on 40nm CMOS technology. The design is implemented using Synopsys Design Compiler, and

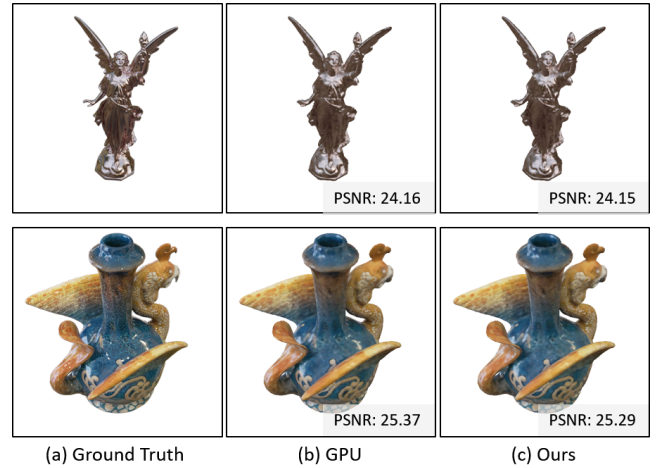


Fig. 14. Comparison of GPU and ICARUS on the SLF rendering task.

power consumption is estimated using Synopsys PrimePower based on real stimulus. To have a comprehensive comparison, we use different implementations of NeRF, including JaxNeRF, which is an optimized version of the original TF NeRF implementation [Deng et al. 2020]. Moreover, we also include implementation results of JaxNeRF using multiple devices.

Table 1 presents the rendering performance comparison of NeRF on different platforms. To the best knowledge of the authors, ICARUS is the first dedicated hardware accelerator design for NeRF-based neural volume rendering tasks. As references, we compare the performance of ICARUS with GPU and TPU, for running the same NeRF algorithm with the same number of sample points per ray.

As we can see, the rendering speed of ICARUS is lower than the TF NeRF and JaxNeRF implementation on a NVIDIA V100 GPU, but the silicon area and power consumption of ICARUS is much smaller.

Table 1. Comparison of NeRF implementation on GPU, TPU and ICARUS

Implementation	TF NeRF [Deng et al. 2020]	JaxNeRF [Deng et al. 2020]			Ours
Platform	NVIDIA V100 \times 1	NVIDIA V100 \times 1	NVIDIA V100 \times 8	TPUv2 \times 128	ICARUS
Process	12 nm			16 nm	40 nm
Clock frequency	1.245 GHz			700MHz	400 MHz
Image resolution	800 \times 800	800 \times 800			800 \times 800
Samples per ray	192	192			192
Time for one frame	27.74 s	20.77 s	2.65 s	0.35 s	45.75 s
Silicon area	815 mm ²		815 mm ² \times 8	611 mm ² \times 128	16.5 mm ²
Power	300 W (TDP)		300 W \times 8 (TDP)	280 W \times 128 (TDP)	282.8 mW
Energy-efficiency	-	-	-	-	0.105 μ J/sample

Energy-efficiency of other implementations is not given due to the lack of run-time power.

Moreover, the CMOS fabrication process we used is two generations older than that of GPU and TPUv2. We also note that the current implementation of ICARUS is running at a much lower clock frequency, i.e., 400MHz, which can be further improved through circuit-level optimization. It should be noted that as commercial products, GPU and TPU include many extra modules to support different applications. While on the other hand, ICARUS is a dedicated hardware architecture tailored for NeRF-type rendering. Therefore, it is hard to have a precise comparison for energy and (silicon) area efficiency since we cannot exclude unnecessary parts in the evaluation for GPU and TPU.

6 DISCUSSION AND FUTURE WORK

Though ICARUS, as a specialized architecture, has advantages in energy and (silicon) area efficiency, there are a number of limitations in our current design. We discuss these limitations and possible solutions to be explored in this section.

Multi-core system. Although PLCores are power-efficient for NeRF rendering, a multi-core system is necessary to meet the requirement of real-time rendering. Due to the volumetric scene representation of NeRF, each sample point in a ray has to go through the pipeline while the processings are independent of one another. Accordingly, the PLCore architecture is designed to independently handle the NeRF processing pipeline of mapping positions & directions to pixel colors. Therefore, NeRF rendering of an image using a multi-core ICARUS can be parallelized with a small overhead of control and off-chip memory exchange. But since all PLCores share the same data path that communicates with DRAM as shown in Fig. 3, the bandwidth of data path may become the bottleneck of the overall system as the number of core increased. Therefore, a memory architecture as well as a network-on-chip that not only provide sufficient data bandwidth for the multi-core system but also minimize the memory access should be carefully designed to support a multi-core ICARUS system.

Fixed-point representation and computation. In our ICARUS design, we use the fixed-point number system, i.e., we convert a NeRF model pre-trained on GPUs to its fixed-point version to ICARUS via quantization. Such post-training quantization will inevitably introduce extra errors, leading to rendering quality degradation as shown in Fig. 12. Therefore, it is essential to explore quantization-aware training techniques [Jacob et al. 2018] that have previously shown great success on CNN models. Specifically, once we manage to integrate quantization into the training process, we will be able to search for the lowest bit-width of the weights of the MLP as we expect them to change under different complexity of the scene in both geometry and appearance. For example, our SLF rendering assumes known geometry and therefore the bit-width should be shorter than traditional NeRF. To that end, an extension to the ICARUS architecture that supports dynamic precision will greatly benefit computational efficiency and rendering quality in the final rendering.

Flexibility vs. efficiency. The neural rendering field has reignited interests on designing new data structures and scene representations. In fact we have observed significant and even accelerated efforts on improving the training and rendering sides of the neural radiance fields. Despite their heterogeneity in algorithm designs (e.g., spatial hashing vs. spatial embedding vs. Octree), it seems that two key components are still shared across all techniques, i.e., positional encoding (PE) and an MLP, shallow or deep. Recall that our ICARUS architecture does not aim for a fixed design. Rather, it hopes to support new configurations by recycling many key implementations such as the PEU and the MLP modules. In fact, the SLF render precisely demonstrates the possibility of combining auxiliary neural networks as well as the possibility of integrating directly into the GPU. Latest extensions to NeRF such as pure MLP based SIGNET [Feng and Varshney 2021] for light field rendering can migrate onto ICARUS, with the PEU re-designed to support Gegenbauer Polynomials-based encoding. We also intend to explore

implementing Instant-NGP on ICARUS which requires implementing hash-based encoding on board.

However, it is equally important to point out that tailored designs are not meant to be for general purposes: specially designed ray tracing accelerator will not be able to achieve comparable performance on rasterization tasks. This is the same case for our prototype ICARUS that requires striking a balance between efficiency and flexibility. For ICARUS, our hope is that its lightweight architecture will be more friendly for mobile devices, such as HMDs in AR/VR applications, smartphones, and 3D displays. In these scenarios, achieving photorealistic rendering on a light, small, low power, and most importantly, untethered HMDs are consumer pain points. In fact, it may be possible to couple ICARUS with any existing mobile GPU units where the background can be rendered via rasterization and the foreground via the neural radiance field.

Further extensions. Although ICARUS has largely focused on computer graphics and computer vision tasks, it may also be extended to broader fields such as medical imaging, electron microscopy and tomography, non-line-of-sight (NLOS) imaging, etc. What they share in common is the volume rendering model, core to the neural radiance field and its extensions. In fact volume rendering can be conducted in the Fourier space [Totsuka and Levoy 1993] analogous to tomographic approaches in CT/MRI/EM/ET. For example, we are currently exploring neural CT reconstruction algorithms as well as how to export them onto ICARUS to support real-time slicing and volume rendering. Many NLOS imaging techniques have also followed the tomographic pipeline and require real-time scene recovery and rendering where neural approaches have emerged as a potential solution. But we understand that proper changes in different parts of ICARUS are necessary to support these aforementioned applications. Decisions need to be made upon the requirement of specific applications. We hope ICARUS will stimulate significant future developments for and beyond graphics and vision.

ACKNOWLEDGMENTS

This work was supported by the Central Guided Local Science and Technology Foundation of China (YDZX202231000010001).

REFERENCES

- Tomas Akenine-Möller, Eric Haines, and Naty Hoffman. 2019. *Real-time rendering*. Crc Press.
- Mike Bailey. 2007. Gsl geometry shaders. *Oregon State University* (2007).
- Chris Buehler, Michael Bosse, Leonard McMillan, Steven Gortler, and Michael Cohen. 2001. Unstructured lumigraph rendering. In *Proceedings of the 28th annual conference on Computer graphics and interactive techniques*. 425–432.
- Edwin Earl Catmull. 1974. *A subdivision algorithm for computer display of curved surfaces*. The University of Utah.
- Anpei Chen, Minye Wu, Yingliang Zhang, Nianyi Li, Jie Lu, Shenghua Gao, and Jingyi Yu. 2018. Deep surface light fields. *Proceedings of the ACM on Computer Graphics and Interactive Techniques* 1, 1 (2018), 1–17.
- Tianshi Chen, Zidong Du, Ninghui Sun, Jia Wang, Chengyong Wu, Yunji Chen, and Olivier Temam. 2014a. DianNao: A Small-Footprint High-Throughput Accelerator for Ubiquitous Machine-Learning. 42, 1 (feb 2014), 269–284. <https://doi.org/10.1145/2654822.2541967>
- Yunji Chen, Tao Luo, Shaoli Liu, Shijin Zhang, Liqiang He, Jia Wang, Ling Li, Tianshi Chen, Zhiwei Xu, Ninghui Sun, and Olivier Temam. 2014b. DaDianNao: A Machine-Learning Supercomputer. In *2014 47th Annual IEEE/ACM International Symposium on Microarchitecture*. 609–622. <https://doi.org/10.1109/MICRO.2014.58>
- Yu-Hsin Chen, Tushar Krishna, Joel S. Emer, and Vivienne Sze. 2017. Eyeriss: An Energy-Efficient Reconfigurable Accelerator for Deep Convolutional Neural Networks. *IEEE Journal of Solid-State Circuits* 52, 1 (jan 2017), 127–138. <https://doi.org/10.1109/JSSC.2016.2616357> arXiv:1512.04295
- Yu-Hsin Chen, Tien-Ju Yang, Joel Emer, and Vivienne Sze. 2019. Eyeriss v2: A Flexible Accelerator for Emerging Deep Neural Networks on Mobile Devices. *IEEE Journal on Emerging and Selected Topics in Circuits and Systems* 9, 2 (2019), 292–308. <https://doi.org/10.1109/JETCAS.2019.2910232>
- Boyang Deng, Jonathan T. Barron, and Pratul P. Srinivasan. 2020. *JaxNeRF: an efficient JAX implementation of NeRF*. <https://github.com/google-research/google-research/tree/master/jaxnerf>.
- Kangle Deng, Andrew Liu, Jun-Yan Zhu, and Deva Ramanan. 2022. Depth-supervised nerf: Fewer views and faster training for free. In *Proceedings of the IEEE/CVF Conference on Computer Vision and Pattern Recognition*. 12882–12891.
- Zidong Du, Robert Fasthuber, Tianshi Chen, Paolo Ienne, Ling Li, Tao Luo, Xiaobing Feng, Yunji Chen, and Olivier Temam. 2015. ShiDianNao: Shifting Vision Processing Closer to the Sensor (ISCA '15). Association for Computing Machinery, New York, NY, USA, 92–104. <https://doi.org/10.1145/2749469.2750389>
- Brandon Y. Feng and Amitabh Varshney. 2021. SIGNET: Efficient Neural Representations for Light Fields. In *International Conference on Computer Vision (ICCV 2021)*.
- Stephan J Garbin, Marek Kowalski, Matthew Johnson, Jamie Shotton, and Julien Valentin. 2021. Fastnerf: High-fidelity neural rendering at 200fps. *arXiv preprint arXiv:2103.10380* (2021).
- Dongsu Han. 2007. Tessellating and Rendering Bezier/B-Spline/NURBS Curves and Surfaces using Geometry Shader in GPU. *University of Pennsylvania* (2007).
- Tom's hardware. 2020. *AMD to Introduce New Next-Gen RDNA GPUs in 2020, Not a Typical 'Refresh' of Navi*. <http://www.tomshardware.com/news/amds-navi-to-be-refreshed-with-next-gen-rdna-architecture-in-2020>
- Benoit Jacob, Skirmantas Kligys, Bo Chen, Menglong Zhu, Matthew Tang, Andrew Howard, Hartwig Adam, and Dmitry Kalenichenko. 2018. Quantization and Training of Neural Networks for Efficient Integer-Arithmetic-Only Inference. In *Proceedings of the IEEE Conference on Computer Vision and Pattern Recognition (CVPR)*.
- Jihyuck Jo, Soyoung Cha, Dayoung Rho, and In-Cheol Park. 2018. DSIP: A Scalable Inference Accelerator for Convolutional Neural Networks. *IEEE Journal of Solid-State Circuits* 53, 2 (2018), 605–618. <https://doi.org/10.1109/JSSC.2017.2764045>
- Norman P. Jouppi, Cliff Young, Nishant Patil, David Patterson, Gaurav Agrawal, Raminder Bajwa, Sarah Bates, Suresh Bhatia, Nan Boden, Al Borchers, Rick Boyle, Pierre-luc Cantin, Clifford Chao, Chris Clark, Jeremy Coriell, Mike Daley, Matt Dau, Jeffrey Dean, Ben Gelb, Tara Vazir Ghaemmaghami, Rajendra Gottipati, William Gulland, Robert Hagmann, C. Richard Ho, Doug Hogberg, John Hu, Robert Hundt, Dan Hurt, Julian Ibarz, Aaron Jaffey, Alek Jaworski, Alexander Kaplan, Harshit Khaitan, Daniel Killebrew, Andy Koch, Naveen Kumar, Steve Lacy, James Laudon, James Law, Dienthu Le, Chris Leary, Zhuoyuan Liu, Kyle Lucke, Alan Lundin, Gordon MacKean, Adriana Maggiore, Maire Mahony, Kieran Miller, Rahul Nagarajan, Ravi Narayanaswami, Ray Ni, Kathy Nix, Thomas Norrie, Mark Omernick, Narayana Penukonda, Andy Phelps, Jonathan Ross, Matt Ross, Amir Salek, Emad Samadiani, Chris Severn, Gregory Sizikov, Matthew Snelham, Jed Souter, Dan Steinberg, Andy Swing, Mercedes Tan, Gregory Thorson, Bo Tian, Horia Toma, Erick Tuttle, Vijay Vasudevan, Richard Walter, Walter Wang, Doug Wilcox, and Doe Hyun Yoon. 2017. In-Datacenter Performance Analysis of a Tensor Processing Unit. In *Proceedings of the 44th Annual International Symposium on Computer Architecture* (Toronto, ON, Canada) (ISCA '17). Association for Computing Machinery, New York, NY, USA, 1–12. <https://doi.org/10.1145/3079856.3080246>
- J. T. Kajiya and H. B. Von. 1984. Ray tracing volume densities" computer graphics 18. (1984).
- Maxim Kazakov. 2007. Catmull-Clark subdivision for geometry shaders. In *Proceedings of the 5th international conference on Computer graphics, virtual reality, visualisation and interaction in Africa*. 77–84.
- Hong-Yun Kim, Young-Jun Kim, and Lee-Sup Kim. 2012. MRTP: Mobile Ray Tracing Processor With Reconfigurable Stream Multi-Processors for High Datapath Utilization. *IEEE Journal of Solid-State Circuits* 47, 2 (2012), 518–535. <https://doi.org/10.1109/JSSC.2011.2171417>
- Hong-Yun Kim, Young-Jun Kim, Jie-Hwan Oh, and Lee-Sup Kim. 2013. A Reconfigurable SMT Processor for Mobile Ray Tracing With Contention Reduction in Shared Memory. *IEEE Transactions on Circuits and Systems I: Regular Papers* 60, 4 (2013), 938–950. <https://doi.org/10.1109/TCSI.2012.2209302>
- Daofu Liu, Tianshi Chen, Shaoli Liu, Jinhong Zhou, Shengyuan Zhou, Olivier Temam, Xiaobing Feng, Xuehai Zhou, and Yunji Chen. 2015. PuDianNao: A Polyvalent Machine Learning Accelerator (ASPLOS '15). Association for Computing Machinery, New York, NY, USA, 369–381. <https://doi.org/10.1145/2694344.2694358>
- Lingjie Liu, Jiatuo Gu, Kyaw Zaw Lin, Tat-Seng Chua, and Christian Theobalt. 2020. Neural sparse voxel fields. *arXiv preprint arXiv:2007.11571* (2020).
- Haimin Luo, Anpei Chen, Qixuan Zhang, Bai Pang, Minye Wu, Lan Xu, and Jingyi Yu. 2021. Convolutional Neural Opacity Radiance Fields. *arXiv preprint arXiv:2104.01772* (2021).
- N. Max. 1995. Optical models for direct volume rendering. *IEEE Transactions on Visualization and Computer Graphics* 1, 2 (1995), 99–108. <https://doi.org/10.1109/2945.468400>

- Daniel Meister, Shinji Ogaki, Carsten Benthin, Michael J Doyle, Michael Guthe, and Jiri Bittner. 2021. A Survey on Bounding Volume Hierarchies for Ray Tracing. In *Computer Graphics Forum*, Vol. 40. Wiley Online Library, 683–712.
- Ben Mildenhall, Pratul P Srinivasan, Matthew Tancik, Jonathan T Barron, Ravi Ramamoorthi, and Ren Ng. 2020. Nerf: Representing scenes as neural radiance fields for view synthesis. In *European conference on computer vision*. Springer, 405–421.
- Bert Moons and Marian Verhelst. 2017. An Energy-Efficient Precision-Scalable ConvNet Processor in 40-nm CMOS. *IEEE Journal of Solid-State Circuits* 52, 4 (2017), 903–914. <https://doi.org/10.1109/JSSC.2016.2636225>
- Thomas Müller, Alex Evans, Christoph Schied, and Alexander Keller. 2022. Instant Neural Graphics Primitives with a Multiresolution Hash Encoding. *arXiv preprint arXiv:2201.05989* (2022).
- Thomas Müller, Alex Evans, Christoph Schied, and Alexander Keller. 2022. Instant Neural Graphics Primitives with a Multiresolution Hash Encoding. *ACM Trans. Graph.* 41, 4, Article 102 (July 2022), 15 pages. <https://doi.org/10.1145/3528223.3530127>
- Jae-Ho Nah, Jin-Woo Kim, Junho Park, Won-Jong Lee, Jeong-Soo Park, Seok-Yoon Jung, Woo-Chan Park, Dinesh Manocha, and Tack-Don Han. 2015. HART: A Hybrid Architecture for Ray Tracing Animated Scenes. *IEEE Transactions on Visualization and Computer Graphics* 21, 3 (2015), 389–401.
- Jae-Ho Nah, Hyuck-Joo Kwon, Dong-Seok Kim, Cheol-Ho Jeong, Jinhong Park, Tack-Don Han, Dinesh Manocha, and Woo-Chan Park. 2014. RayCore: A Ray-Tracing Hardware Architecture for Mobile Devices. *ACM Trans. Graph.* 33, 5, Article 162 (sep 2014), 15 pages. <https://doi.org/10.1145/2629634>
- Jae-Ho Nah, Jeong-Soo Park, Chanmin Park, Jin-Woo Kim, Yun-Hye Jung, Woo-Chan Park, and Tack-Don Han. 2011. T&I Engine: Traversal and Intersection Engine for Hardware Accelerated Ray Tracing. *ACM Trans. Graph.* 30, 6 (dec 2011), 1–10. <https://doi.org/10.1145/2070781.2024194>
- Martin E Newell, RG Newell, and Tom L Sancha. 1972. A solution to the hidden surface problem. In *Proceedings of the ACM annual conference-Volume 1*. 443–450.
- Nvidia. 2020. *NVIDIA Ampere Architecture*. <https://www.nvidia.com/en-us/data-center/ampere-architecture/>
- Jongsun Park, Woopyo Jeong, Hamid Mahmoodi-Meimand, Yongtao Wang, Hunsoo Choo, and Kaushik Roy. 2004. Computation sharing programmable FIR filter for low-power and high-performance applications. *IEEE Journal of Solid-State Circuits* 39, 2 (feb 2004), 348–357. <https://doi.org/10.1109/JSSC.2003.821785>
- Jeong Joon Park, Peter Florence, Julian Straub, Richard Newcombe, and Steven Lovegrove. 2019. DeepSDF: Learning continuous signed distance functions for shape representation. In *Proceedings of the IEEE/CVF conference on computer vision and pattern recognition*. 165–174.
- K. Perlin and E. M. Hoffert. 1989. Hypertexture (SIGGRAPH '89). Association for Computing Machinery, New York, NY, USA, 253–262. <https://doi.org/10.1145/74333.74359>
- Hanspeter Pfister, Jan Hardenbergh, Jim Knittel, Hugh Lauer, and Larry Seiler. 1999. The VolumePro Real-Time Ray-Casting System. In *Proceedings of the 26th Annual Conference on Computer Graphics and Interactive Techniques (SIGGRAPH '99)*. ACM Press/Addison-Wesley Publishing Co., USA, 251–260. <https://doi.org/10.1145/311535.311563>
- Nasim Rahaman, Aristide Baratin, Devansh Arpit, Felix Draxler, Min Lin, Fred Hamprecht, Yoshua Bengio, and Aaron Courville. 2019. On the spectral bias of neural networks. In *International Conference on Machine Learning*. PMLR, 5301–5310.
- Christian Reiser, Songyou Peng, Yiyi Liao, and Andreas Geiger. 2021. KiloNeRF: Speeding up Neural Radiance Fields with Thousands of Tiny MLPs. *arXiv preprint arXiv:2103.13744* (2021).
- VV Sanzharov, Vladimir A Frolov, and Vladimir A Galaktionov. 2020. Survey of Nvidia RTX Technology. *Programming and Computer Software* 46, 4 (2020), 297–304.
- Jörg Schmittler, Ingo Wald, and Philipp Slusallek. 2002. SaarCOR: A Hardware Architecture for Ray Tracing. In *Proceedings of the ACM SIGGRAPH/EUROGRAPHICS Conference on Graphics Hardware (Saarbrücken, Germany) (HWW'02)*. Eurographics Association, Goslar, DEU, 27–36.
- Josef Spjut, Andrew Kensler, Daniel Kopta, and Erik Brunvand. 2009. TRaX: A Multicore Hardware Architecture for Real-Time Ray Tracing. *IEEE Transactions on Computer-Aided Design of Integrated Circuits and Systems* 28, 12 (2009), 1802–1815.
- Cheng Sun, Min Sun, and Hwann-Tzong Chen. 2021. Direct Voxel Grid Optimization: Super-fast Convergence for Radiance Fields Reconstruction. *arXiv preprint arXiv:2111.11215* (2021).
- Matthew Tancik, Pratul Srinivasan, Ben Mildenhall, Sara Fridovich-Keil, Nithin Raghavan, Utkarsh Singhal, Ravi Ramamoorthi, Jonathan Barron, and Ren Ng. 2020. Fourier features let networks learn high frequency functions in low dimensional domains. *Advances in Neural Information Processing Systems* 33 (2020).
- Takashi Totsuka and Marc Levoy. 1993. Frequency domain volume rendering. In *Proceedings of the 20th annual conference on Computer graphics and interactive techniques*. 271–278.
- Daniel N Wood, Daniel I Azuma, Ken Aldinger, Brian Curless, Tom Duchamp, David H Salesin, and Werner Stuetzle. 2000. Surface light fields for 3D photography. In *Proceedings of the 27th annual conference on Computer graphics and interactive techniques*. 287–296.
- Sven Woop. 2007. A programmable hardware architecture for realtime ray tracing of coherent dynamic scenes. *Diss. Ph. D. Thesis, Sarrland University* (2007).
- Sven Woop, Jörg Schmittler, and Philipp Slusallek. 2005. RPU: A Programmable Ray Processing Unit for Realtime Ray Tracing. *ACM Trans. Graph.* 24, 3 (jul 2005), 434–444. <https://doi.org/10.1145/1073204.1073211>
- Shouyi Yin, Peng Ouyang, Shibin Tang, Fengbin Tu, Xiudong Li, Shixuan Zheng, Tianyi Lu, Jiangyuan Gu, Leibo Liu, and Shaojun Wei. 2018a. A High Energy Efficient Reconfigurable Hybrid Neural Network Processor for Deep Learning Applications. *IEEE Journal of Solid-State Circuits* 53, 4 (2018), 968–982. <https://doi.org/10.1109/JSSC.2017.2778281>
- Shouyi Yin, Peng Ouyang, Jianxun Yang, Tianyi Lu, Xiudong Li, Leibo Liu, and Shaojun Wei. 2018b. An Ultra-High Energy-Efficient Reconfigurable Processor for Deep Neural Networks with Binary/Ternary Weights in 28NM CMOS. In *2018 IEEE Symposium on VLSI Circuits*. 37–38. <https://doi.org/10.1109/VLSIC.2018.8502388>
- Shouyi Yin, Peng Ouyang, Shixuan Zheng, Dandan Song, Xiudong Li, Leibo Liu, and Shaojun Wei. 2018c. A 141 UW, 2.46 PJ/Neuron Binarized Convolutional Neural Network Based Self-Learning Speech Recognition Processor in 28NM CMOS. In *2018 IEEE Symposium on VLSI Circuits*. 139–140. <https://doi.org/10.1109/VLSIC.2018.8502309>
- Alex Yu, Sara Fridovich-Keil, Matthew Tancik, Qinhong Chen, Benjamin Recht, and Angjoo Kanazawa. 2021a. Plenoxels: Radiance Fields without Neural Networks. *arXiv preprint arXiv:2112.05131* (2021).
- Alex Yu, Ruilong Li, Matthew Tancik, Hao Li, Ren Ng, and Angjoo Kanazawa. 2021b. Plenotrees for real-time rendering of neural radiance fields. *arXiv preprint arXiv:2103.14024* (2021).
- Huangjie Yu, Anpei Chen, Xin Chen, Lan Xu, Ziyu Shao, and Jingyi Yu. 2022. Anisotropic Fourier Features for Neural Image-Based Rendering and Relighting. In *Proceedings of the AAAI Conference on Artificial Intelligence*.
- Ellen D Zhong, Tristan Bepler, Joseph H Davis, and Bonnie Berger. 2019. Reconstructing continuous distributions of 3D protein structure from cryo-EM images. *arXiv preprint arXiv:1909.05215* (2019).